

# Synthesizing Speech from Intracranial Depth Electrodes using an Encoder-Decoder Framework

Jonas M. Kohler<sup>1</sup> | Maarten C. Ottenhoff<sup>2</sup> | Sophocles Goulis<sup>2</sup> | Miguel Angrick<sup>3</sup> | Albert J. Colon<sup>5</sup> | Louis Wagner<sup>5</sup> | Simon Tousseyn<sup>5</sup> | Pieter L. Kubben<sup>2,4</sup> | Christian Herff<sup>2</sup>

<sup>1</sup>Department of Computer Science, ETH Zurich, Switzerland

<sup>2</sup>Department of Neurosurgery, School of Mental Health and Neurosciences, Maastricht University, Maastricht, Netherlands

<sup>3</sup>Cognitive Systems Lab, University of Bremen, Bremen, Germany

<sup>4</sup>Academic Center for Epileptology, Kempenhaeghe/Maastricht University Medical Center, location Maastricht, Netherlands

<sup>5</sup>Academic Center for Epileptology, Kempenhaeghe/Maastricht University Medical Center, location Kempenhaeghe, Netherlands

## Correspondence

Christian Herff, Maastricht University  
Email: c.herff@maastrichtuniversity.nl

## Funding information

C.H. acknowledges funding by the Dutch Research Council (NWO) through the research project 'Decoding Speech In sEEG (DESI)' with project number VI.Veni.194.021.

Speech Neuroprostheses have the potential to enable communication for people with dysarthria or anarthria. Recent advances have demonstrated high-quality text decoding and speech synthesis from electrocorticographic grids placed on the cortical surface. Here, we investigate a less invasive measurement modality, namely stereotactic EEG (sEEG) that provides sparse sampling from multiple brain regions, including subcortical regions. To evaluate whether sEEG can also be used to synthesize high-quality audio from neural recordings, we employ a recurrent encoder-decoder framework based on modern deep learning methods. We demonstrate that high-quality speech can be reconstructed from these minimally invasive recordings, despite a limited amount of training data. Finally, we utilize variational feature dropout to successfully identify the most informative electrode contacts.

## KEYWORDS

**Abbreviations:** BCI, Brain-Computer Interface; iEEG, intracranial Electroencephalography; sEEG, stereotactic Electroencephalography.

## 1 | INTRODUCTION

Brain-Computer Interfaces have progressed tremendously over the last decade and now enable patients who have lost the ability to communicate due to injury, stroke or neuromuscular disorders, using a robotic arm [1], high-performance cursor control [2] or even imagined handwriting [3] with information transfer rates up to approximately 12 bits/second. Without a doubt, this ability to restore communication through typing or writing improves the quality of life of patients drastically. However, the potential of BCIs does not stop here. In fact, an active line of research is pushing technology for speech decoding from neural signals, as spoken language is still our most natural form of communication with bit rates around 39 bits/second across many languages [4].

Several approaches to directly decode speech from invasive measures of brain activity have been presented in recent years [5, 6]. Martin et al. [7] decoded spectro-temporal features of speech from electrocorticographic (ECoG) electrodes placed on the cortical surface. In [8], Lotte et al. showed that articulatory features of speech could be decoded from ECoG recordings, which was later investigated in more depth in [9]. Mugler et al. [10] demonstrated that the full set of American English phonemes can be decoded from ECoG. Combining these decoding successes with approaches from Automatic Speech Recognition (ASR), Herff et al. [11] and Moses et al. [12] presented that a textual representation of continuous speech could be reliably decoded from ECoG. Moses et al. even demonstrated their approach in real-time [13, 14]. Decoding a textual representation of speech has the potential to help patients communicate with friends and family again. However, crucial information is lost in the textual representation such as intonation, prosody and accentuation. To give patients access to the full expressive power of speech, direct synthesis of speech from neural data is better suited.

The aforementioned systems employ various machine learning approaches. Artificial Neural networks have provided breakthrough results in a variety of scientific domains. The temporal structure and complex auto-correlations of both neural dynamics and speech are best captured using recurrent neural networks that incorporate sequential information through feedback connections. Two recent studies demonstrated that non-recurrent neural networks can also be employed to synthesize produced [15] and perceived [16] speech from ECoG recordings. Berezutskaya et al. [17] used recurrent neural networks to predict neural activity from sound features of perceived audio. Makin et al. [18] employed an encoder-decoder framework to decode a textual representation of speech from ECoG recordings. In a break-through study [19], a closed-loop version of this approach was even used by a patient suffering from anarthria. Instead of a textual representation, Anumachipalli et al. [20] decoded articulatory gestures from ECoG and translated these gestures into an audio waveform.

All approaches previously discussed utilize brain activity that is measured directly on the cortical surface with ECoG electrodes. These electrodes require a large craniotomy. In the monitoring of epilepsy patients, in which almost all of the previous studies have been conducted, more and more centers utilize the less invasive stereotactic EEG (sEEG), which is measured with intracranial depth electrodes [21]. The use of sEEG for BCI has been discussed before [22] and one study demonstrates that imagined speech can be synthesized in real-time from sEEG recordings [23]. However, the authors opted for an overly simple decoding pipeline that does not respect the temporal nature of the problem and hence only produces low-quality, unintelligible speech output.

Here, we employ a large neural network architecture that naturally leverage chronological relations to demonstrate the feasibility of speech neuroprostheses based on sEEG by producing very high-quality audio output. For this purpose, we apply an encoder decoder architecture with attention mechanisms [24] to create audible speech from neural recordings with intracranial depth electrodes. To ensure physiological feasibility of the decoding algorithms, we employ variational feature dropout on the trained models to identify the most information bearing electrode contacts and demonstrate that decoding is also possible using this smaller subset of electrodes. We believe that this explainability mechanism increases a potential translation of neural network based speech neuroprostheses into viable products as it allows for a more targeted location selection with a reduced overall number of implanted electrodes.

## 2 | MATERIAL & METHODS

### 2.1 | Experimental Setup

**Participants** Three patients (20, 59, and 40 years old, two male, one female) suffering from intractable epilepsy participated in our experiment. All patients were native speakers of Dutch. Patients were implanted with depth electrodes to identify the epileptic foci and plan potential resections. During this mapping procedure, patients participated voluntarily in our experiment and provided written informed consent. The experiment was conducted in accordance with the declaration of Helsinki and approved by the IRB of both Maastricht University and the Epilepsy Center Kempenhaeghe.

**Experiment and Data Recording** Participants were shown a total of 100 sentences from the Mozilla Common Voice Dutch corpus [25] on a computer screen in front of them. All sentences were selected to be between 5 and 7 words long and displayed in pseudo-randomized order. Each sentence was followed by a 2-second rest interval during which a fixation cross was shown on the screen. Duration of each sentence depended on the participants' reading speed leading to total recording lengths between 10 and 20 minutes.

Neural data were sampled at either 1024 Hz or 2048 Hz using a Micromed SD LTM amplifier (Micromed S.p.A., Treviso, Italy). Electrodes were referenced to a common white matter electrode contact. Speech data was recorded using the experiment laptop's in-build microphone and sampled at 48 kHz. Neural data, audio data and the experiment timings were synchronized using LabStreamingLayer [26]. Data for this study is available at <https://osf.io/7wf6n/>.

**Electrode Localization** Electrode number and locations were purely determined based on clinical necessity. Electrodes with a total of 117, 111 and 127 contacts were implanted for participants 1, 2 and 3, respectively. Electrode locations were identified using `img_pipe` [27] after co-registering pre-surgical T1-weighted MR scans with post-surgical CT scans. Anatomical labels were acquired from Freesurfer's [28] cortical parcellation.

**Data Processing** Speech signals were recorded at 48 kHz and downsampled to 22'050 Hz using a pre-computed (kaiser best) filter implemented in LibROSA [29]. For each 12.5 ms block of the recorded speech, we perform a short time Fourier transformation with corresponding re-scaling to obtain a mel-spectrogram representation which is spectrally normalized in a final step using dynamic range compression. All steps follow the procedure from Shen et al. [30], in which 80 mel frequency coefficients between 0 and 8000 Hz are calculated.

We limited our analysis of the sEEG data to the high-gamma band between 70 and 170 Hz, which is routinely employed in studies decoding speech from intracranial recordings [20, 16, 23] as it contains speech [31, 32] and language

[33] specific information. The specificity of the high-gamma signal might be explained through the high correlation with ensemble spiking [34] and can also be used to identify speech articulatory gestures [9] and smiling [35] from intracranial recordings. The high-gamma band was extracted using an IIR bandpass filter with filter order 8. The first two harmonics of the line noise (50Hz) were attenuated using elliptic IIR notch filters (filter order 8). We then estimated the signal envelope using the absolute of the Hilbert envelope.

## 2.2 | Decoding Model

Our model is composed of a recurrent sequence-to-sequence feature prediction network, that maps neural activity to mel-scale spectrograms, and a neural vocoder that synthesizes time-domain waveforms from the generated spectrograms. While the first component is largely inspired by the Tacotron-2 model [30], which is mainly used in text to speech synthesis tasks, the latter component is a flow based generative model termed WaveGlow [36], which we use without modifications. Figure 1 depicts our model in its entirety. Source code for the neural network models as well as some audio samples can be found at <https://github.com/jonaskohler/stereoEEG2speech>.

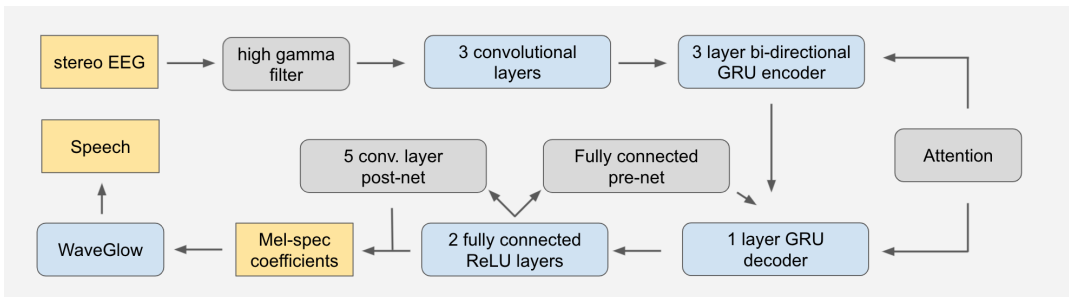


**FIGURE 1 Model overview:** Our pipeline consists of two major parts, as indicated by the yellow squares. The first transforms sEEG inputs into time-aligned mel-spectrogram coefficients and is trained end-to-end as detailed out in Section 2.2.1. The second uses the pre-trained WaveGlow vocoder [36] without any modifications to generate speech.

### 2.2.1 | Spectrogram regression

On a high level, the spectrogram regression consists of two major steps. We first feed the high gamma band of the neural activity into a convolutional neural network with one dimensional kernels. This networks acts as a filter that learns meaningful latent representations of the input, which are then fed into an RNN encoder-decoder. This latter network is tasked with mapping the convolved input sequence to a target output sequence of mel spectral coefficients.

The initial mapping setup is done in a sliding window approach. To be precise, we process the continuous input sequence windows of 400ms which we slide trough the input with a hop of 25ms (Fig. 2) . For each window, we add an additional 400ms of sEEG signal before and after the actual speech to account for mental processes like speech planning and understanding. In the testing phase, audio windows are non-overlapping.

**CNN** First, the convolutional neural networks (CNN) receives sequences of neural activity across all channels at 1024 khz. This signal is being convolved in three layers with decreasing kernel size and increasing number of channels to

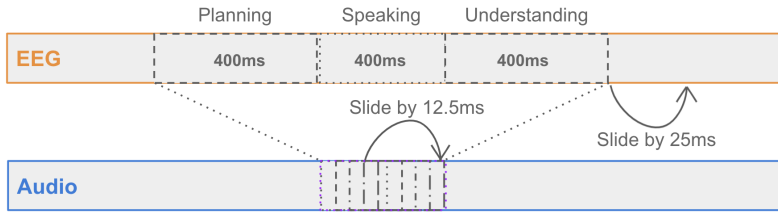


**FIGURE 2 Sliding window approach (Training):** We

process the continuous input sequence windows of 400ms which we slide through the input with a hop of 25ms. For each window, we add an additional 400ms of sEEG signal before and after the actual speech to account for mental processes like speech planning and understanding. Within each audio window, we perform a short time Fourier transformation with corresponding re-scaling to obtain a mel-spectrogram representation of each 12.5 ms block.

result in an output of dimensionality 300 across 100Hz. All layers use Batch Normalization [37] and ReLU activation functions. One dimensional max pooling is applied in the last layer.

**RNN** Secondly, we add positional embeddings to the convolved input sequence [24], reverse its time order and then feed it into a three-layer bi-directional RNN encoder with gated recurrent units [38]. The encoder converts this sequence into a hidden feature representation of dimensionality 333, which the decoder consumes to predict a spectrogram in an autoregressive manner (i.e. one step at a time). In this typical encoder-decoder setting, the information of the entire input sequence is compressed into a single fixed-length vector, which makes it hard for the decoder to cope with long input sequences. As our sEEG input sequences are much longer than for example sentences in natural language, we employ an additive attention mechanism termed Bahdnav-Attention [39] which allows the decoder to attend to the hidden states of any time step of the input sequence separately.

Inspired by Tacotron-2, the decoder output is post-processed by a set of two linear layers (pre-net), which act as an information bottleneck, before it is fed back into the decoder as initial state for the next timestep. Furthermore, while the decoder output is concatenated to the attention context vector and projected through a linear transform to predict the target spectrogram frame as usual, it is also passed through a 5-layer convolutional post-net which predicts a residual to add to the prediction to improve the overall reconstruction.

**Training** We train the feature extractor (CNN) and spectrogram predictor (RNN) in an end-to-end fashion, applying the standard maximum-likelihood training procedure with a mean-squared-error loss and a teacher forcing ratio of 0.1. That is, in 10% of the cases we replace the decoder prediction from the previous state with the ground truth. We employ the AdamW optimizer with default parameters [40], batch-size 512 and (grid-searched) learning rate  $\eta = 0.0005$  as well as a weight decay of  $\lambda = 0.001$ . We train for a fixed number of 50 epochs and employ a learning rate scheduler which decreases  $\eta$  by a factor of two in epoch 45. Our architecture has a total of  $10'411'964$  trainable parameters.

To be precise, our model transforms a sequence of sEEG input with  $c$  channels  $\mathbf{X} \in \mathbb{R}^{c \times T_1}$  into a sequence of 80

dimensional mel spectrogram coefficients  $\hat{\mathbf{Y}} \in \mathbb{R}^{80 \times T_2}$  and minimizes

$$\mathcal{L}(\mathbf{W}) = \frac{1}{2} \|\mathbf{Y} - \hat{\mathbf{Y}}\|_F^2, \quad \hat{\mathbf{Y}} := f_{NN}(\mathbf{X}, \mathbf{W}), \quad (1)$$

where  $\mathbf{Y} \in \mathbb{R}^{80 \times T_2}$  contains the ground truth mel-coefficients and  $f_{NN} : \mathbb{R}^{c \times T_1} \rightarrow \mathbb{R}^{80 \times T_2}$  represents the network mapping which is parametrized by a set of weights  $\mathbf{W}$ . The specific values  $T_1$  and  $T_2$  are determined by the window- and hop size with which we move through the data ( $T_1$ ) as well as by the interval in which we compute mel spectrograms ( $T_2$ ). See Fig. 2) for an illustration.

**Feature ranking** In order to identify regions of the brain that are particularly useful for further developments of speech BCIs, we use a recent method called variational feature dropout [41] to quantify the importance of each of the  $\sim 100$  electrode contacts in the input signal. This technique is particularly attractive as it is model agnostic and thus easy to employ even in more complex neural network architectures such as the one employed in this study (see Fig. 1). In a nutshell, given a trained model, variational feature dropout adds a dropout layer with trainable dropout rates to the input and fine-tunes the model with an additional regularization term in the loss functions that incentivizes large accumulated dropout rates. The trade-off between the original loss and the new regularizer pushes the optimizer to increase dropout probabilities for unimportant features while keeping those of relevant features low.

In our specific case, we re-parametrize  $\mathbf{X}^k := \mathbf{Z}\mathbf{X}$ , with  $\mathbf{Z} := \text{diag}(z_1^k, \dots, z_c^k)$  in each iteration  $k$ , where

$$z_j^k = \phi\left(\frac{1}{t} \left( \log(\theta_j) - \log(1 - \theta_j) + \log(u_j^k) - \log(1 - u_j^k) \right)\right), \quad (2)$$

$u_j^k \sim \mathcal{U}[0, 1]$ ,  $t = 0.1$  (smoothing parameter) and  $\phi(\cdot)$  represents the sigmoid function. As a result, instead of drawing  $z_j^k \in [0, 1]$  directly from a Bernoulli distribution  $p(z|\theta)$ , we sample from a continuous relaxation that allows for backpropagation through the dropout rates  $\theta$  (see [42] for details). We then augment the loss function given in Eq.(1) by a variational regularizer  $r(\mathbf{Z}) = \lambda \text{Tr}(\mathbf{Z})$ ,  $\lambda > 0$  which incentivizes the dropout frequency of unimportant features. Finally, we run 10 additional epochs with the same hyperparameter setting as detailed above in order to rank the sEEG channels by the predictive importance.

Subsequently, we identify the top 33 most relevant electrode contacts and re-train the networks from scratch using just these 33 features in order to sanity check the learned feature ranking. Indeed, as detailed out in the following Section, the predictive performance of our sequence to sequence model drops only slightly after discarding more then two thirds of the sEEG channels.

**Baseline Comparison** To establish whether the proposed model outperforms previously described approaches, we compare our results to a synthesis approach based on a densely connected CNN presented in [15]. We follow exactly the implementations detailed there. The architecture is composed of densely connected convolutional blocks and transition blocks in an alternating manner (see Fig. 3 in the original paper). Contrary to our Encoder-Decoder network, we feed windows of 50ms length into this network as this is what the network architecture was optimized for in the original work. Also along the lines of [15], we split the channel dimension into two to generate (preferably) square

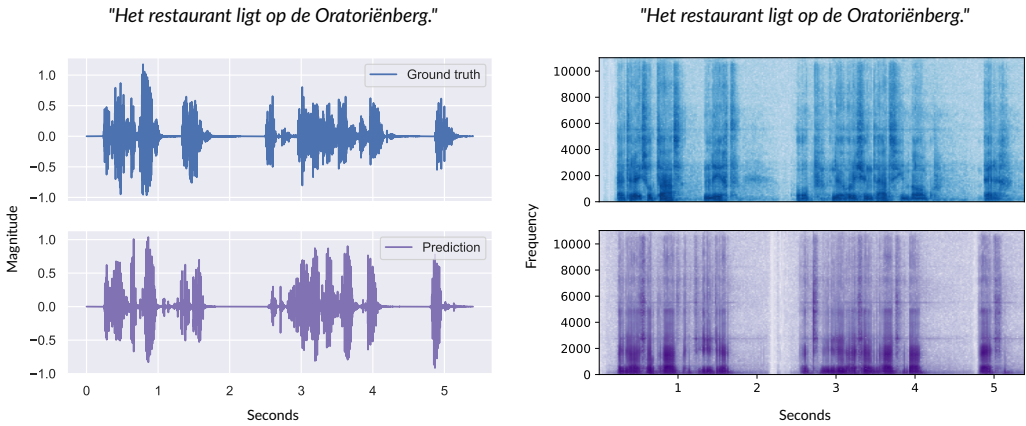


**FIGURE 3** An exemplary sentence (5.5 seconds) from the test set of patient 3 in waveform (left) and spectrogram (right) representation.

two dimensional inputs for each time step (network employs three dimensional convolutional kernels). To ensure comparability between the two approaches, we feed in original time series, as we do for the recurrent architecture, instead of averages in windows as utilized in the original study. Our implementation of the baseline system has 86'020 trainable parameters.

### 2.2.2 | Speech generation

After completing the first step of transforming sEEG signal to mel-spectrograms, we employ a flowbased generative model to turn these time-aligned features into an audio waveform. Specifically, we employ Nvidia's WaveGlow model [36], which is designed to provide fast, efficient and high-quality audio synthesis without the need for auto-regression, as a plug and play decoder to synthesize speech. As a sanity check, we compare original audio recordings from the training set to generated audio samples and found that WaveGlow provides decent quality speech. We proceed equally here for both the proposed encoder decoder architecture as well as the baseline from [15].

## 3 | RESULTS

### 3.1 | High quality speech is generated from intracranial depth electrodes

We employed a fixed training-validation-test split, where both the validation and test set have a fixed length of 1.5 minutes for each set and patient. The remaining data were used as training set, whose specific length per patient is given in the first column of Table 1.

Our method produces audio waveforms that are very similar to the ground truth (see Figure 3 for a particularly successful sentence of Patient 3). When first primed with the ground truth, the generated audio is sometimes even

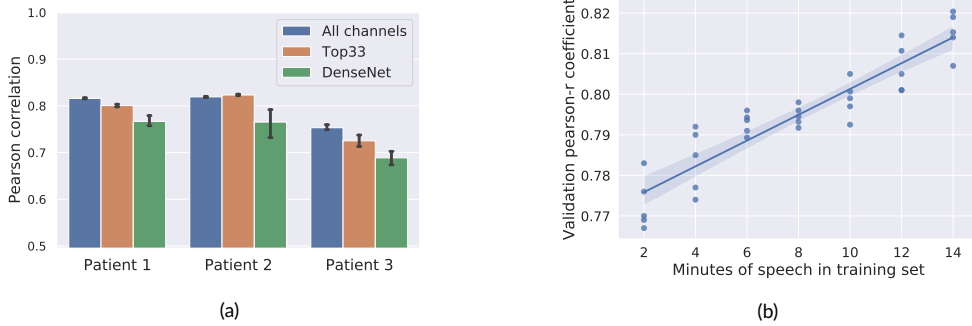


**FIGURE 4** Pearson correlation results on the test set. (A) Pearson correlation coefficient for different settings and patients. Mean and 95% confidence interval of 5 independent runs. The proposed methods outperforms the DenseNet baseline for all three patients. The selected subset of features yields only minor deterioration in results, if any. (B) Correlation coefficients for patient 2 on training sets of increasing length. Five independent runs for each setting. Results still increase with large training set sizes suggesting that improved results can be expected when more data is available.

comprehensible<sup>1</sup>. Additionally, the combination of the encoder-decoder framework with the WaveGlow vocoder succeeds in preserving voice characteristics to a remarkable degree. These results demonstrate that intracranial depth electrodes can be used to synthesize high-quality audio, despite the suboptimal sampling across many brain regions instead of the focused sampling of relevant areas provided by ECoG.

	Training		Validation		Test		
	All channels	Top33	All channels	Top33	All channels	Top33	DenseNet
Patient 1 (7min)	0.24 ±0.02	0.26 ±0.04	1.9 ±0.2	2.6 ±0.3	<b>2.1±0.1</b>	2.9 ±0.1	7.4 ±2.0
Patient 2 (14min)	0.4 ±0.01	0.41 ±0.03	1.5 ±0.2	2.2 ±0.2	<b>1.8 ±0.1</b>	2.4 ±0.2	10.3 ±3.1
Patient 3 (17min)	0.31 ±0.02	0.35 ±0.03	1.3 ±0.1	2.0 ±0.2	<b>1.4 ±0.2</b>	2.1 ±0.3	7.1 ±2.7

**TABLE 1** Mean-squared error loss of our model with all - and 33 most relevant channels as found by variational feature dropout (Section 2.2.1) as well as DenseNet baseline from [15]. Mean ( $\pm$  standard deviation) of five independent random initializations.

Our approach outperforms the baseline from [15] both in terms of mean-squared-error loss (Tab. 1) and Pearson correlation coefficient (Fig. 4 (a)). The proposed recurrent encoder-decoder architecture explicitly uses the temporal nature of both the neural as well as the audio data and is thereby better able to capture the intricate temporal dynamics.

It is important to note the very limited amount of training data in this setting. The longest recording (patient 3) only contains 17 minutes of training data, of which more than half is silence. We explored the influence of training set size on reconstruction quality (Fig. 4 (b)) and observed a clear improvement with more training data. Given the large amount of trainable parameters, it is not surprising that our architecture can still benefit from more training data. The fact that reconstruction quality does not plateau gives rise to the hope that improved results can be expected with more training data.

<sup>1</sup>audio samples can be found here: <https://github.com/jonaskohler/stereoEEG2speech>



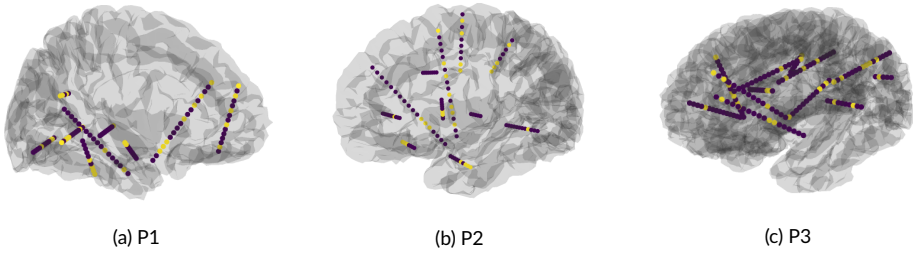


**FIGURE 5** Electrode contact locations (purple) and selected top 33 electrode contacts (yellow) for all participants. Electrode locations are determined by co-registering pre-surgical MRI and post-surgical CT scans.

To investigate the most contributing brain regions, we identified the 33 most important electrode contacts. Subsequently, we retrained the model with just this subset of electrode contacts. Performance drops only slightly for patient 1 and 3 and even improves for patient 2 (Tab. 1 and Fig. 4 (a)). This is likely due to the drastic decrease in dimensionality of the input space. The reduced number of necessary electrode contacts make the vision of a fully implanted neuroprosthesis for patients more feasible, as less electrodes would need to be implanted.

### 3.2 | Wide network of brain regions contribute to decoding

Electrode locations are purely determined by clinical need and are not influenced by our study. This leads to vastly different coverage for each individual patient (Fig. 5). Patient 1 was implanted with electrodes on the right hemisphere, patient 2 on the left and patient 3 received bilateral electrodes. Using the variational feature dropout, we identified the electrode contacts that provide most information to the decoding process. (Fig. 5 contacts highlighted in yellow). The implanted electrodes sample neural data from a large variety of cortical and sub-cortical regions including many which are associated with speech production, such as: inferior and middle frontal gyrus, insular, central sulcus, superior temporal gyrus and sulcus. The most information-rich contacts appear in a variety of these regions, but also often lie within the white matter. This is in line with recent studies that have observed meaningful information within the white matter [43] and have found white matter contacts beneficial for decoding problems [44]. While speech is often considered to be left hemisphere dominant in most people, right hemisphere involvement has been reported [45, 46] and can explain the decoding success for patient 1 with only right hemisphere electrodes.

### 3.3 | Temporal Context is similar in audio and neural data

Fig. 6 visualizes attention matrices which illustrate the temporal context in the encoder ( $x$ -axis) that the decoder ( $y$ -axis) attends to. This temporal context appears to be well aligned between neural data and corresponding audio, which is shown by the diagonal structure of the high attention scores (bright colors). No high attentions scores are present in the early and late parts of the encoder sequence, suggesting that the padding of additional 400 ms before and after the targeted speech segment might not be necessary. This is somewhat contradictory to prior investigation in the temporal context of speech production [47], but can be explained by the recurrent nature of our reconstruction model. As the sequence to sequence model incorporates the temporal structure of the data, smaller context might

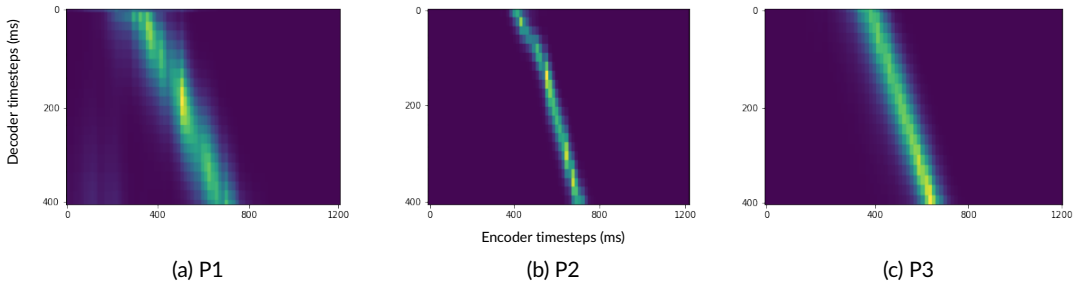


**FIGURE 6** Attention matrix visualizing attention scores at convergence of three different runs (brighter values indicate higher attention scores). Time steps in the decoder are depicted on the y-axis, encoder timesteps are depicted on the x-axis. The diagonal structure suggests that the attention scores are well aligned in the time domain, as for example latter steps in the output attend to latter steps in the input. The figure is furthermore suggestive of the fact that padding the input sEEG sequence (speech planning and understanding) might be unnecessary, as not much attention is paid to the very first and very last input steps.

be necessary to include the complete information.

## 4 | DISCUSSION

In this study, we demonstrated that minimally invasive recordings of neural activity can be used to synthesize high-quality audio, despite the suboptimal sampling of distributed brain regions. The similarity of the procedure to implantation of deep brain stimulation electrodes, which are routinely implanted for many years, gives hope for the feasibility in patient cohorts [22]. By investigating the most information-bearing regions, we could show that multiple brain regions contribute to the decoding and that there is not a single clear area that is required to decode speech processes. This is explainable by the large amount of regions involved in speech perception [48] and production [49]. Recent findings identify more and more brain areas involved in these intricate processes, including for example the hippocampus [50].

Despite the very promising results achieved with our approach, it is important to note that all results were produced on previously recorded, offline data of patients that were speaking audibly. Furthermore, the long temporal context used in our approach combined with the long processing time of our encoder-decoder framework prevent our approach from being applicable to a real-time scenario. With this, the approach has some of the inherent disadvantages of approaches that decode a textual representation of speech [12, 18, 11], namely that they cannot provide the natural flow of a conversation. To enable this, real-time synthesis of neural data is necessary [23]. Our results on the temporal context of the architecture point out that shorter temporal contexts might suffice, bringing us closer to real-time readiness. The employed WaveGlow architecture for reconstruction of audio waveforms from spectral representation is already real-time ready. Our approach does capture the participants' own voice and is potentially capable of reconstructing speech information beyond the words, such as prosody and accentuation.

In the data presented here, participants spoke naturally. For a speech neuroprosthesis to be useful to patients, it needs to function on imagined or attempted speech processes. Two studies have investigated decoding textual representations from attempted speech [19] and speech synthesis from imagined speech [23]. Investigating attempted

of imagined speech processes without immediate feedback is challenging, so it is outside of the scope of this first feasibility study for high-quality reconstruction from sEEG.

Compared to standard text-to-speech (TTS) approaches, our approach is trained on tiny amounts of relatively noisy data. Our analysis (Fig. 4 (b)) highlight that results have not saturated yet, and that more training data is still expected to improve reconstruction results. Alternatively, techniques such as data augmentation and ensembling should improve performance. Additionally, fine tuning the speech decoder on our dataset is likely to further improve audio quality, which is a relevant step once speech BCIs approach clinical application.

Despite these limitations, our study demonstrates the large potential of encoder-decoder based deep learning models to produce high-quality speech reconstruction from minimally invasive neural recordings.

## 5 | DATA AND CODE AVAILABILITY

Code used in this study is available on <https://github.com/jonaskohler/stereoEEG2speech>. All data used in this study is available on <https://osf.io/7wf6n/>. Note that the participants' voices are anonymized.

## Acknowledgements

We are grateful to Yannic Kilcher for insightful discussions. C.H. acknowledges funding by the Dutch Research Council (NWO) through the research project 'Decoding Speech In SEEG (DESI)' with project number VI.Veni.194.021.

## references

- [1] Hochberg LR, Bacher D, Jarosiewicz B, Masse NY, Simeral JD, Vogel J, et al. Reach and grasp by people with tetraplegia using a neurally controlled robotic arm. *Nature* 2012;485(7398):372–375.
- [2] Pandarinath C, Nuyujukian P, Blabe CH, Sorice BL, Saab J, Willett FR, et al. High performance communication by people with paralysis using an intracortical brain-computer interface. *Elife* 2017;6:e18554.
- [3] Willett FR, Avansino DT, Hochberg LR, Henderson JM, Shenoy KV. High-performance brain-to-text communication via handwriting. *Nature* 2021 May;593(7858):249–254. <https://doi.org/10.1038/s41586-021-03506-2>.
- [4] Coupé C, Oh YM, Dediu D, Pellegrino F. Different languages, similar encoding efficiency: Comparable information rates across the human communicative niche. *Science advances* 2019;5(9):eaaw2594.
- [5] Herff C, Schultz T. Automatic speech recognition from neural signals: a focused review. *Frontiers in neuroscience* 2016;10.
- [6] Chakrabarti S, Sandberg HM, Brumberg JS, Krusienski DJ. Progress in speech decoding from the electrocorticogram. *Biomedical Engineering Letters* 2015;5(1):10–21.
- [7] Martin S, Brunner P, Holdgraf C, Heinze HJ, Crone NE, Rieger J, et al. Decoding spectrotemporal features of overt and covert speech from the human cortex. *Frontiers in Neuroengineering* 2014;7(14).
- [8] Lotte F, Brumberg JS, Brunner P, Gunduz A, Ritaccio AL, Guan C, et al. Electrocorticographic representations of segmental features in continuous speech. *Frontiers in human neuroscience* 2015;9.

- [9] Chartier J, Anumanchipalli GK, Johnson K, Chang EF. Encoding of articulatory kinematic trajectories in human speech sensorimotor cortex. *Neuron* 2018;98(5):1042–1054.
- [10] Mugler EM, Patton JL, Flint RD, Wright ZA, Schuele SU, Rosenow J, et al. Direct classification of all American English phonemes using signals from functional speech motor cortex. *Journal of neural engineering* 2014;11(3):035015.
- [11] Herff C, Heger D, De Pestera A, Telaar D, Brunner P, Schalk G, et al. Brain-to-text: decoding spoken phrases from phone representations in the brain. *Frontiers in neuroscience* 2015;9:217.
- [12] Moses DA, Mesgarani N, Leonard MK, Chang EF. Neural speech recognition: continuous phoneme decoding using spatiotemporal representations of human cortical activity. *Journal of neural engineering* 2016;13(5):056004.
- [13] Moses DA, Leonard MK, Chang EF. Real-time classification of auditory sentences using evoked cortical activity in humans. *Journal of neural engineering* 2018;15(3):036005.
- [14] Moses DA, Leonard MK, Makin JG, Chang EF. Real-time decoding of question-and-answer speech dialogue using human cortical activity. *Nature communications* 2019;10(1):1–14.
- [15] Angrick M, Herff C, Mugler E, Tate MC, Slutzky MW, Krusienski DJ, et al. Speech synthesis from ECoG using densely connected 3D convolutional neural networks. *Journal of neural engineering* 2019;16(3):036019.
- [16] Akbari H, Khalighinejad B, Herrero JL, Mehta AD, Mesgarani N. Towards reconstructing intelligible speech from the human auditory cortex. *Scientific reports* 2019;9(1):874.
- [17] Berezutskaya J, Freudenburg ZV, Güçlü U, van Gerven MA, Ramsey NF. Brain-optimized extraction of complex sound features that drive continuous auditory perception. *PLoS computational biology* 2020;16(7):e1007992.
- [18] Makin JG, Moses DA, Chang EF. Machine translation of cortical activity to text with an encoder–decoder framework. *Nature neuroscience* 2020;23(4):575–582.
- [19] Moses DA, Metzger SL, Liu JR, Anumanchipalli GK, Makin JG, Sun PF, et al. Neuroprosthesis for Decoding Speech in a Paralyzed Person with Anarthria. *New England Journal of Medicine* 2021;385(3):217–227.
- [20] Anumanchipalli GK, Chartier J, Chang EF. Speech synthesis from neural decoding of spoken sentences. *Nature* 2019;568(7753):493–498. <https://doi.org/10.1038/s41586-019-1119-1>.
- [21] van der Loo LE, Schijns OE, Hoogland G, Colon AJ, Wagner GL, Dings JT, et al. Methodology, outcome, safety and in vivo accuracy in traditional frame-based stereoelectroencephalography. *Acta neurochirurgica* 2017;159(9):1733–1746.
- [22] Herff C, Krusienski DJ, Kubben P. The Potential of Stereotactic-EEG for Brain-Computer Interfaces: Current Progress and Future Directions. *Frontiers in Neuroscience* 2020;14:123.
- [23] Angrick M, Ottenhoff M, Diener L, Ivucic D, Ivucic G, Goulis S, et al. Real-time Synthesis of Imagined Speech Processes from Minimally Invasive Recordings of Neural Activity. *bioRxiv* 2020;.
- [24] Vaswani A, Shazeer N, Parmar N, Uszkoreit J, Jones L, Gomez AN, et al. Attention is all you need. *arXiv preprint arXiv:1706.03762* 2017;.
- [25] Ardila R, Branson M, Davis K, Henretty M, Kohler M, Meyer J, et al. Common voice: A massively-multilingual speech corpus. *arXiv preprint arXiv:1912.06670* 2019;.
- [26] Kothe C. Lab streaming layer (LSL). <https://github.com/sccn/labstreaminglayer> Accessed on October 2014;26:2015.
- [27] Hamilton LS, Chang DL, Lee MB, Chang EF. Semi-automated anatomical labeling and inter-subject warping of high-density intracranial recording electrodes in electrocorticography. *Frontiers in Neuroinformatics* 2017;11:62.
- [28] Fischl B. *FreeSurfer*. *Neuroimage* 2012;62(2):774–781.

- [29] McFee B, Raffel C, Liang D, Ellis DP, McVicar M, Battenberg E, et al. librosa: Audio and music signal analysis in python. In: Proceedings of the 14th python in science conference, vol. 8; 2015. .
- [30] Shen J, Pang R, Weiss RJ, Schuster M, Jaitly N, Yang Z, et al. Natural tts synthesis by conditioning wavenet on mel spectrogram predictions. In: 2018 IEEE International Conference on Acoustics, Speech and Signal Processing (ICASSP) IEEE; 2018. p. 4779–4783.
- [31] Leuthardt E, Pei XM, Breshears J, Gaona C, Sharma M, Freudenburg Z, et al. Temporal evolution of gamma activity in human cortex during an overt and covert word repetition task. *Frontiers in human neuroscience* 2012;6:99.
- [32] Crone N, Hao L, Hart J, Boatman D, Lesser R, Irizarry R, et al. Electrographic gamma activity during word production in spoken and sign language. *Neurology* 2001;57(11):2045–2053.
- [33] Towle VL, Yoon HA, Castelle M, Edgar JC, Biassou NM, Frim DM, et al. ECoG gamma activity during a language task: differentiating expressive and receptive speech areas. *Brain* 2008;131(8):2013–2027.
- [34] Ray S, Crone NE, Niebur E, Franaszczuk PJ, Hsiao SS. Neural correlates of high-gamma oscillations (60–200 Hz) in macaque local field potentials and their potential implications in electrocorticography. *Journal of Neuroscience* 2008;28(45):11526–11536.
- [35] Kern M, Bert S, Glanz O, Schulze-Bonhage A, Ball T. Human motor cortex relies on sparse and action-specific activation during laughing, smiling and speech production. *Communications biology* 2019;2(1):1–14.
- [36] Prenger R, Valle R, Catanzaro B. Waveglow: A flow-based generative network for speech synthesis. In: ICASSP 2019–2019 IEEE International Conference on Acoustics, Speech and Signal Processing (ICASSP) IEEE; 2019. p. 3617–3621.
- [37] Ioffe S, Szegedy C. Batch normalization: Accelerating deep network training by reducing internal covariate shift. In: International conference on machine learning PMLR; 2015. p. 448–456.
- [38] Cho K, Van Merriënboer B, Gulcehre C, Bahdanau D, Bougares F, Schwenk H, et al. Learning phrase representations using RNN encoder-decoder for statistical machine translation. arXiv preprint arXiv:1406.1078 2014;.
- [39] Bahdanau D, Cho K, Bengio Y. Neural machine translation by jointly learning to align and translate. arXiv preprint arXiv:1409.0473 2014;.
- [40] Loshchilov I, Hutter F. Decoupled weight decay regularization. arXiv preprint:1711.05101 2017;.
- [41] Chang CH, Rampasek L, Goldenberg A. Dropout feature ranking for deep learning models. arXiv preprint arXiv:1712.08645 2017;.
- [42] Gal Y, Hron J, Kendall A. Concrete dropout. arXiv preprint arXiv:1705.07832 2017;.
- [43] Mercier MR, Bickel S, Megevand P, Groppe DM, Schroeder CE, Mehta AD, et al. Evaluation of cortical local field potential diffusion in stereotactic electro-encephalography recordings: a glimpse on white matter signal. *Neuroimage* 2017;147:219–232.
- [44] Li G, Jiang S, Paraskevopoulou SE, Chai G, Wei Z, Liu S, et al. Detection of human white matter activation and evaluation of its function in movement decoding using stereo-electroencephalography (SEEG). *Journal of Neural Engineering* 2021;18(4):0460c6.
- [45] Tourville JA, Reilly KJ, Guenther FH. Neural mechanisms underlying auditory feedback control of speech. *Neuroimage* 2008;39(3):1429–1443.
- [46] Alexandrou AM, Saarinen T, Mäkelä S, Kujala J, Salmelin R. The right hemisphere is highlighted in connected natural speech production and perception. *NeuroImage* 2017;152:628–638.

- 
- [47] Brumberg JS, Krusienski DJ, Chakrabarti S, Gunduz A, Brunner P, Ritaccio AL, et al. Spatio-Temporal Progression of Cortical Activity Related to Continuous Overt and Covert Speech Production in a Reading Task. *PLoS one* 2016;11(11):e0166872.
- [48] Hickok G, Poeppel D. Towards a functional neuroanatomy of speech perception. *Trends in cognitive sciences* 2000;4(4):131–138.
- [49] Hickok G. Computational neuroanatomy of speech production. *Nature reviews neuroscience* 2012;13(2):135–145.
- [50] van de Ven V, Waldorp L, Christoffels I. Hippocampus plays a role in speech feedback processing. *NeuroImage* 2020;223:117319.